Paper AIAA 2014-2497 7th AIAA Theoretical Fluid Mechanics Conference, Atlanta GA June 2014

Transient Growth in Hypersonic Boundary Layers

N. P. Bitter* and J. E. Shepherd†

California Institute of Technology, Pasadena, CA, 91125, USA

This paper investigates the relative importance of modal and non-modal growth mechanisms in flat-plate, hypersonic boundary layers as well as the effects of Mach number and wall cooling on these processes. Optimal disturbances are calculated in both the spatial and temporal frameworks using an eigenvector decomposition of the locally-parallel, linearized Navier-Stokes equations. It is found that for every Mach number there is an optimal level of wall cooling that minimizes transient growth; at this condition the wall temperature is slightly below the freestream temperature, with lower wall temperatures needed as the Mach number increases. The competition between modal and non-modal growth mechanisms is examined over a range of Reynolds numbers by calculating N factor curves for both processes. For conditions relevant to high enthalpy flows (high Mach number, cold wall), transient growth is rapidly overtaken by modal instabilities while the level of amplification remains small. At lower Mach numbers or adiabatic conditions, the transient growth is overtaken more slowly. For low Mach numbers and cold walls, no modal instabilities exist, but the level of non-modal amplification is increased such that the initiation of transition by infinitesimal perturbations is plausible despite the absence of modal instabilities.

I. Introduction

UNDERSTANDING and predicting the stability of supersonic and hypersonic boundary layers is necessary for minimizing heat loads and skin friction drag on high speed aircraft and reentry vehicles. Most of the early work in this field emphasized the exponential growth of perturbations corresponding to unstable discrete eigenvalues[1–4], but more recently it has been recognized that non-modal growth mechanisms can lead to large transient amplification of disturbances in spite of their eventual asymptotic decay. It has been hypothesized that this amplification may be sufficient to excite nonlinear interactions which ultimately cause the breakdown into turbulent motion[5,6].

Non-modal growth first received a great deal of attention in the incompressible flow regime[5,7–11] since it provides a plausible explanation for the experimentally observed transition of flows that are linearly stable.[12,13] The first transient growth analysis of compressible boundary layers was conducted by Hanifi et al. using the temporal framework.[14] They found that the optimal disturbances in compressible boundary layers share many features with those in incompressible ones; for instance, optimal perturbations take the form of streamwise vortices, energy growth scales with the Reynolds number based on x, and the amplification is driven by Landahl's "lift-up" effect[15,16]. Subsequent compressible transient-growth analyses have employed the spatial framework[17] and focused on the inclusion of nonparallel flow effects[18–20].

As discussed by Corbett[21] for the incompressible case, flows can experience a competition between modal and non-modal growth mechanisms. At low enough Reynolds numbers, the flow is generally modally stable and the only possible growth mechanism is non-modal, which may or may not produce large amounts of amplification depending on the flow conditions. At higher Reynolds numbers, both modal and non-modal growth mechanisms may be active, and one must determine whether the short-time dynamics of transient growth are able to surpass the exponential amplification of unstable modes. The first objective of this paper is to map out regions in the parameter space over which modal or non-modal mechanisms are dominant, considering in particular the effects of Mach number, Reynolds number, and wall temperature.

In comparing the amplification caused by modal and non-modal mechanisms, the wall temperature condition and Mach number are of great importance. It is well-known that the growth rates of both the first

*PhD Candidate, Graduate Aeronautical Laboratories, 1200 E. California Blvd. MC 105-50

†Professor, Graduate Aeronautical Laboratories, 1200 E. California Blvd. MC 105-50, AIAA Member.

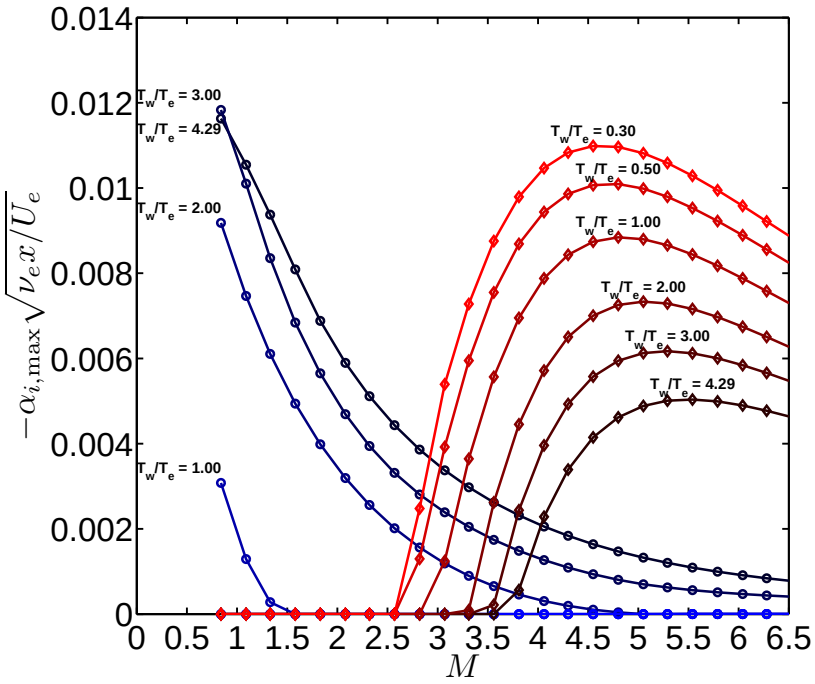

Figure 1. Effect of wall temperature on spatial growth rates of first and second instability modes. Reynolds number is $R_\delta = \sqrt{U_e x/\nu_e} = 1500$. Blue ($-\circ-$) and red ($-\diamond-$) curves correspond to the first and second modes. For all curves, the growth rate is optimized over all frequencies ω and all wave angles ψ with respect to the streamwise direction. The first mode is stable for cases having $T_w/T_e = 0.3$ and 0.5.

and second mode instabilities are quite sensitive to these parameters[2,3,22], the first mode being stabilized by wall cooling and the second and higher modes being destabilized. These trends are demonstrated in Fig. 1, in which the maximum spatial growth rates for the first and second modes are plotted as functions of Mach number and level of wall cooling. The technique (to be published) used to produce this plot employs the shooting method developed by Mack[1] and has been validated by reproducing the work of several other researchers for flat plate boundary layers[3,23–25]. Figure 1 shows that as the level of wall cooling is increased, the second mode growth rate is significantly increased, and the Mach number at which the second mode "cuts in" becomes smaller. Figure 1 also demonstrates a substantial reduction in first mode growth rate as the wall is cooled, a finding which was first predicted (in the inviscid limit) by Lees and Lin[26,27]. Lines for the first mode instability with $T_w/T_e = 0.3$ and 0.5 are not included on the plot because the first mode is stable at those conditions.

Although the influence of wall cooling is well-known for modal instabilities, with regard to transient growth the effects of wall cooling are not so simple and have not been studied in great detail. Tumin et al.[17,18] did investigate the effects of wall cooling for relatively low Mach numbers of 0.5 and 3.0 as well as modest levels of wall cooling (T_w/T_{ad} = 0.25-1.0), and they observed a reduction in transient growth with wall cooling for $M = 3$ and an increase for $M = 0.5$. Tempelmann et al.[20] also investigated the effect of wall cooling for a swept flat-plate boundary layer at $M = 0.75$ and found wall cooling to increase the level of transient growth, which is consistent Tumin's result. Reshotko and Tumin[28] reported a wider range of wall temperatures and Mach numbers and demonstrated that the wall temperature effect is strongly dependent on the Mach number. In this paper, a systematic study of the effects of Mach number and wall temperature is undertaken to further clarify the roles of these parameters in transient growth.

The previously-mentioned transient growth studies have, for the most part, considered only relatively modest levels of wall cooling ($T_w/T_{ad} = 0.25 - 1.0$). However when experiments are conducted in high enthalpy impulse facilities, the temperature ratio may be much smaller. In such facilities the wall temperature is typically ambient and the freestream temperature is on the order of 1000-2500 K, which leads to wall temperature ratios in the range of $T_w/T_{ad} = 0.02 - 0.1$ at about $M = 5$. At these conditions the ratio of wall temperature to edge temperature is $T_w/T_e = 0.1 - 0.3$, so on the basis of Fig. 1 the first mode instability is expected to be absent while the second mode is highly unstable for high Mach numbers. The transient growth

response of boundary layers under such conditions is not known, so our present study seeks to evaluate the non-modal growth and compare it with the amplification caused by the highly unstable second mode.

An interesting feature of Fig. 1 is the absence of modal instabilities for flows with a cold wall and $M < 2.5$. At these conditions, the first mode is stable because of the high level of wall cooling and the second mode is stable because of the low Mach number. The absence of modal instabilities raises the question of whether or not such boundary layers are completely stable to infinitesimal perturbations, with transition to turbulence being caused only by nonlinear interactions between finite amplitude disturbances. In this paper we investigate whether transient growth produces sufficient amplification to plausibly lead to transition in such flows.

The transient growth calculations reported in this paper are conducted mainly in the temporal framework, but we also report several cases in the spatial framework as well. Although previous research has been done in both the temporal[14,29] and spatial[17,18,20] cases, the connection between the two frameworks remains unclear and few direct comparisons between the two methods are available. Several authors[30,31] have reported promising results in which spatial results are nearly reproduced from the temporal ones by a simple re-scaling of variables; however, an analogue to the Gaster transform that might facilitate the comparison between spatial and temporal results has not yet been proposed. Nevertheless, by comparing the results of the references above it is clear that the spatial and temporal calculations have the same qualitative behavior, including the form of the optimal perturbations, the magnitude of energy growth achieved, the scaling of results with Reynolds and Mach numbers, and the effects of wall-cooling. In this study, we make both spatial and temporal transient growth calculations for selected cases that are otherwise identical in order to clarify the similarities and differences between the two methods.

II. Methodology

II.A. Mean Flow Calculation

The mean flow is modeled using a similarity solution based on the method of Klunker and McLean[32] which is able to incorporate arbitrary fluid transport properties so long as they depend only on the temperature. This is the case when the flow is either in thermochemical equilibrium or thermochemically frozen. The effects of chemical reactions are beyond the scope of the present paper, so we focus on low and moderate enthalpy flows where chemical reactions are negligible. The mean flow is assumed to be in vibrational equilibrium (thermally perfect gas), and the variation of specific heats with temperature is modeled by treating the diatomic gas as a system of harmonic oscillators[33]. All simulations reported in this paper assume air as the test gas. The viscosity is calculated using Sutherland's formula and the thermal conductivity is modeled by Euken's method[33].

The boundary layer equations of continuity, momentum, and energy for a compressible viscous flow over a flat plate are the following:

$$\frac{\partial}{\partial x^*}(\rho^* u^*) + \frac{\partial}{\partial y^*}(\rho^* v^*) = 0 \tag{1a}$$

$$\rho^* u^* \frac{\partial u^*}{\partial x^*} + \rho^* v^* \frac{\partial u^*}{\partial y^*} = \frac{\partial}{\partial y^*}\left(\mu^* \frac{\partial u^*}{\partial y^*}\right) \tag{1b}$$

$$\rho^* u^* \frac{\partial h^*}{\partial x^*} + \rho^* v^* \frac{\partial h^*}{\partial y^*} = \frac{\partial}{\partial y^*}\left(k^* \frac{\partial T^*}{\partial y^*}\right) + \mu^* \left(\frac{\partial u^*}{\partial y^*}\right)^2 \tag{1c}$$

where ρ is the density, p the pressure, (u, v) the velocity components, μ the shear viscosity, h the enthalpy, and asterisks denote dimensional quantities. These equations are made dimensionless using the following definitions:

$$(u, v) = \frac{(u^*, v^*)}{U_e} \quad (x, y) = \frac{(x^*, y^*)}{\delta} \quad p = \frac{p^*}{\rho_e U_e^2} \quad \rho = \frac{\rho^*}{\rho_e} \quad \mu = \frac{\mu^*}{\mu_e} \quad \Theta = \frac{h - h_e}{0.5 U_e^2} \quad \sigma = \frac{c_p^* \mu^*}{k^*} \tag{2}$$

Here δ is the Blasius length scale $\delta = \sqrt{\nu_e x / U_e}$ and subscripts 'e' denote the edge conditions. Additionally, a similarity variable η is defined by

$$\eta = \frac{y^*}{x^*}\sqrt{\frac{U_e x^*}{\nu_e}} \tag{3}$$

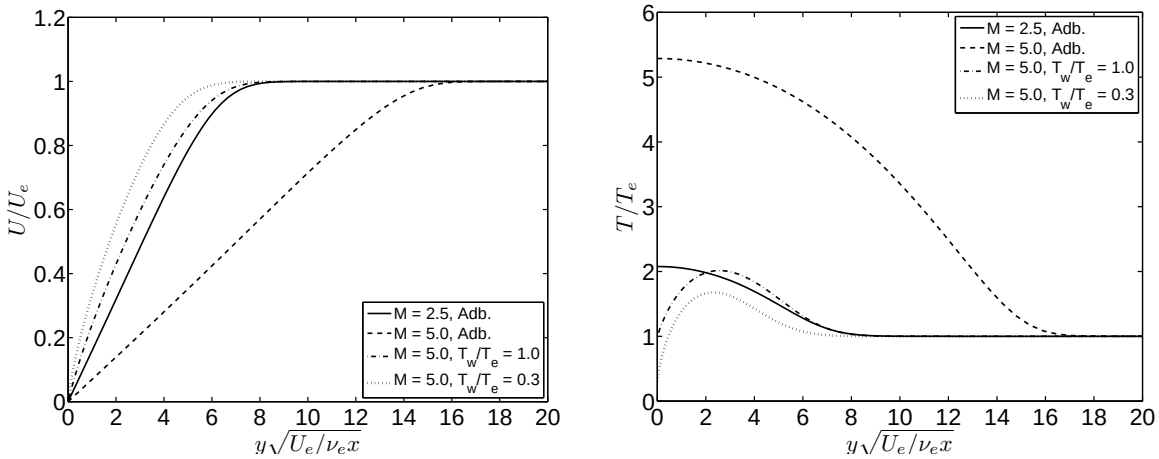

Figure 2. Mean profiles of velocity (left) and temperature (right) for several Mach numbers and wall temperature conditions.

Substitution of the above dimensionless variables into (1) and elimination of the vertical velocity via the continuity equation leads to a pair of ordinary differential equations in terms of the similarity variable η:

$$g\frac{du}{d\eta} + \frac{d}{\eta}\left(\mu\frac{du}{d\eta}\right) = 0 \tag{4}$$

$$g\frac{d\Theta}{d\eta} + \frac{1}{\sigma_e}\frac{d}{d\eta}\left(\frac{\mu}{\sigma}\frac{d\Theta}{d\eta}\right) = -2\mu\left(\frac{du}{d\eta}\right)^2 \tag{5}$$

where g is defined by

$$g = \frac{1}{2}\int_0^\eta (\rho u)d\eta' \tag{6}$$

These equations are solved by the method of successive approximations as described by Klunker and McLean[32]; the incompressible Blasius boundary layer is used as an initial guess and the velocity and enthalpy distributions are iteratively refined until the RMS error of both the velocity and enthalpy profiles falls below 10^{-9}. Examples of several velocity and temperature profiles determined in this manner are shown in Fig. 2.

II.B. Global Eigenvalue Calculation

The calculation of the global eigenvalue spectrum is based on the single-domain spectral collocation method of Malik[34]. The term "global" here refers to the fact that the method produces a discrete approximation to the entire eigenvalue spectrum, as opposed to "local" methods which determine a single eigenvalue at a time. To begin with, the relevant flow variables are assumed to take the form:

$$\begin{pmatrix} u \\ v \\ p \\ T \\ w \end{pmatrix} = \begin{pmatrix} \bar{U}(y) \\ 0 \\ \bar{P} \\ \bar{T}(y) \\ 0 \end{pmatrix} + \begin{pmatrix} \hat{u}(y) \\ \hat{v}(y) \\ \hat{p}(y) \\ \hat{\theta}(y) \\ \hat{w}(y) \end{pmatrix} \times \exp\left(i\alpha x + i\beta z - i\omega t\right) \tag{7}$$

where x, y, and z are the streawise, wallnormal, and spanwise directions. The flow is assumed to be locally parallel, meaning that the mean-flow variables, designated $\bar{(\cdot)}$, are functions only of y and the vertical velocity of the mean flow is neglected. This assumption has been evaluated by Tumin and Reshotko[18], who demonstrated that the inclusion of non-parallel effects leads to some quantitative differences in the maximum transient growth but little qualitative change in the behavior; they concluded that "nonparallel effects probably are not significant for estimates of transient growth." Since in this paper we are interested mainly in qualitative trends and orders of magnitude, the slight numerical errors introduced by the locally parallel flow assumption are deemed acceptable.

When the Navier-Stokes equations have been linearized with respect to the perturbation quantities, designated $\hat{(\cdot)}$, the result can be expressed as a 5×5 system:

$$\left(\mathbf{A}\mathcal{D}^2 + \mathbf{B}\mathcal{D} + \mathbf{C}\right)\hat{\mathbf{q}} = 0 \qquad\qquad \hat{\mathbf{q}} = \left[\hat{u}, \hat{v}, \hat{p}, \hat{\theta}, \hat{w}\right] \tag{8}$$

Here $\mathcal{D}$ is the derivative operator with respect to y and $\mathbf{A}$, $\mathbf{B}$, and $\mathbf{C}$ are matrices that are listed by Malik[34]. The derivative operators $\mathcal{D}$ are approximated using collocated Chebyshev differentiation matrices based on N collocation points placed at the Gauss-Lobatto quadrature nodes[35]. The resulting system is expressed in the form of a generalized eigenvalue problem

$$\left(\mathbb{A}_o + \mathbb{A}_\omega\omega + \mathbb{A}_{\alpha 1}\alpha + \mathbb{A}_{\alpha 2}\alpha^2\right)\hat{\mathbf{q}} = 0 \tag{9}$$

where $\mathbb{A}_o$, $\mathbb{A}_\omega$, $\mathbb{A}_{\alpha 1}$, and $\mathbb{A}_{\alpha 2}$ are all $5N \times 5N$ matrices. For a temporal analysis, the value of α is prescribed and matrices $\mathbb{A}_o$, $\mathbb{A}_{\alpha 1}$, and $\mathbb{A}_{\alpha 2}$ are combined leaving a generalized eigenvalue problem for ω. For a spatial analysis the value of ω is prescribed, leaving a quadratic eigenvalue problem for α. Unless otherwise stated, the quadratic term is neglected to produce a linear eigenvalue problem. This approximation is appropriate since the optimal disturbances are characterized by very small streamwise wavenumbers. However, in a few instances we also solve the full, quadratic eigenvalue problem to verify that the linearization is acceptable. In these cases, the quadratic problem is solved by introducing the additional variables $\alpha\hat{u}$, $\alpha\hat{v}$, $\alpha\hat{\theta}$, and $\alpha\hat{w}$, which allows an equivalent $9N \times 9N$ linear eigenvalue problem to be constructed using the method of Malik[34]. For both the linear and quadratic problems, eigenvectors and eigenvalues of the system are calculated using the LAPACK implementation of the QZ algorithm. This global eigenvalue calculation has been verified by reproducing the test cases of Malik[34] and the eigenvalue spectra of Hanifi et al.[14]

II.C. Transient Growth Calculation

The transient growth calculation used in this paper closely follows the method of Hanifi et al.[14] Denoting the eigenvectors of (9) by $\tilde{\mathbf{q}}$, the disturbance vector $\mathbf{q}$ is projected onto the truncated eigenvector space as follows:

$$\mathbf{q} = \sum_{k=1}^{N} \kappa_k \tilde{\mathbf{q}}_k(y) e^{-i\omega_k t} \tag{10}$$

where κ_k are expansion coefficients. For spatial analysis, the argument of the exponential is replaced by $i\alpha_k x$. The eigenvector decomposition may be represented compactly in vector notation by the relation

$$\mathbf{q} = \mathbf{Q}\mathbf{\Lambda}\boldsymbol{\kappa} \tag{11}$$

where $\mathbf{Q}$ is a matrix containing the eigenvectors $\tilde{\mathbf{q}}_k$ as its columns, $\mathbf{\Lambda}$ is the diagonal matrix having diagonal elements $\exp(i\omega_k t)$ or $\exp(i\alpha_k x)$, and $\boldsymbol{\kappa}$ is the column vector of expansion coefficients. The disturbance norm selected for evaluation of energy growth is

$$2E = \int_0^{y_{\max}} \bar{\rho}\left(|\hat{u}|^2 + |\hat{v}|^2 + |\hat{w}|^2\right) + \frac{\bar{T}}{\gamma\bar{\rho}M^2}|\hat{\rho}|^2 + \frac{\bar{\rho}}{\gamma(\gamma-1)\bar{T}M^2}|\hat{\theta}|^2 dy \tag{12}$$

This norm was proposed by Mack[2] in the context of modal instability and was later re-derived by Hanifi et al.[14] by requiring that pressure work be conservative. An excellent description of this energy norm is also provided by Chu[36]. The energy norm can be written in terms of the eigenvector expansion (11) as follows:

$$2E = (\mathbf{\Lambda}\boldsymbol{\kappa})^H \left[\int_0^{y_{\max}} \mathbf{Q}^H\mathbf{M}\mathbf{Q} dy\right] \mathbf{\Lambda}\boldsymbol{\kappa} \tag{13}$$

where superscript H designates the Hermitian transpose and $\mathbf{M}$ is a 5×5 matrix containing the coefficients of the disturbance quantities in (12). The integral in brackets is a positive-definite matrix, thus it may be factored as the product of a matrix $\mathbf{F}$ and its Hermitian transpose[37]:

$$\mathbf{F}^H\mathbf{F} \equiv \int_0^{y_{\max}} \mathbf{Q}^H\mathbf{M}\mathbf{Q} dy \tag{14}$$

The matrix $\mathbf{F}$ can be calculated using the Cholesky decomposition; this matrix does not depend on time or on the eigenvector expansion coefficients $\boldsymbol{\kappa}$, so it can be immediately computed once the eigenvector basis is known. By combining the definition in (14) with (13), the energy norm can be written as a weighted 2-norm of the expansion coefficients $\boldsymbol{\kappa}$:

$$2E = (\mathbf{F\Lambda\kappa})^H(\mathbf{F\Lambda\kappa}) = ||\mathbf{F\Lambda\kappa}||_2^2 \tag{15}$$

The energy amplification G is then

$$G \equiv \max \frac{E}{E(0)} = \max \frac{||\mathbf{F\Lambda\kappa}||_2^2}{||\mathbf{F\kappa}||_2^2} = \max \frac{||\mathbf{F\Lambda F^{-1}F\kappa}||_2^2}{||\mathbf{F\kappa}||_2^2} = ||\mathbf{F\Lambda F^{-1}}||_2^2 \tag{16}$$

The 2-norm of this matrix is calculated using the singular value decomposition, and the eigenvector expansion coefficients $\boldsymbol{\kappa}$ of the optimal perturbation are extracted from right singular vector corresponding to the largest singular value[37]. For the temporal case, $G(\alpha, \beta, t)$ is the maximum possible amplification that can occur at time t for a given combination of values of α and β. Likewise, for a spatial analysis $G(\alpha, \beta, x)$ is the maximum amplification that can occur a distance x downstream of the initial station. Following the notation of Hanifi et al.[14], the maximum value of G over all values of t (temporal case) or x (spatial case) will be denoted $G_{\max}(\alpha, \beta)$, and the value of $G_{\max}$ that is optimized over all values of α and β will be referred to as G_{opt}. This quantity can be regarded as a property of the boundary layer. The time or distance at which the optimal amplification is achieved is denoted t_{opt} or x_{opt}, and the optimal spanwise wavenumber is denoted β_{opt}.

The numerical implementation of the transient growth calculation is as follows. For a chosen pair of wavenumbers (α, β), the global eigenvalue spectrum is computed as described in Sec. II.B. In all calculations, the number of grid points is 150, the height of the domain is $y_{\max} = 100$, and half of the grid points are clustered below $y = 10$ using the algebraic grid stretching suggested by Malik[34]. We have performed pointwise checks at a large number of different conditions using 100 or 200 grid points as well as domain heights of 100, 200, or 300, and have found that the values of $G_{\max}$ are affected less than 0.5% by these changes, which confirms that the transient growth calculation is converged.

If any unstable modes are found in the global eigenvalue calculation, they are refined using a local stability solver similar to that of Mack[1]. The difference between the eigenvalue from the global calculation and the local refinement is typically less than 0.1%, which provides further validation of our technique since the same result is obtained by two independent methods. If unstable modes are present, the calculation is terminated since the maximum energy growth is then infinite. If no unstable modes are found by the global eigenvalue calculation, then the matrix $\mathbf{F}$ defined in (14) is constructed from the eigenvector basis. The numerical integration involved in (14) is carried out using the spectrally accurate method reported in the appendix of Hanifi et al.[14] Having constructed the matrix $\mathbf{F}$ and its inverse, the product $\mathbf{F\Lambda F^{-1}}$ is formed for different values of time t (or x for spatial analysis) and for each value of t the singular value decomposition is employed to obtain G. This procedure is repeated until the time t is found that maximizes G.

The transient growth calculation described here has been validated by reproducing both the temporal results of Hanifi et al.[14] and the spatial results of Tumin[17]. An example of the comparison with Tumin's work is shown in Fig. 3, where good agreement is seen over a wide range of Mach numbers.

III. Results

III.A. Optimal Perturbations

Figure 4 shows contour plots of the maximum temporal energy amplification, $G_{\max}$, as a function of streamwise and spanwise wavenumber. Each plot is constructed on a grid of 150 values each of α and β. The Mach numbers are 2.5 (left) and 5.0 (right), the wall is adiabatic, and the Reynolds number based on boundary layer thickness is $R_\delta \equiv \sqrt{U_e x/\nu_e} = \sqrt{Re_x} = 300$. The colored contours represent $G_{\max}(\alpha, \beta)$, but the white regions contain unstable modes and hence the maximum possible energy amplification in these zones is infinite. Contour lines in these regions instead indicate the temporal growth rate, ω_i, with contour lines equally spaced between zero and the maximum value, which is reported in Table 1. The unstable regions that are visible in Fig. 4 correspond to the first mode instability and have their maximum growth rate for $\beta > 0$, indicating that oblique disturbances are most unstable. The second mode is also unstable at this Reynolds number for $M = 5$, but the instability region is located at $\alpha > 0.1$ and is not visible on the plot.

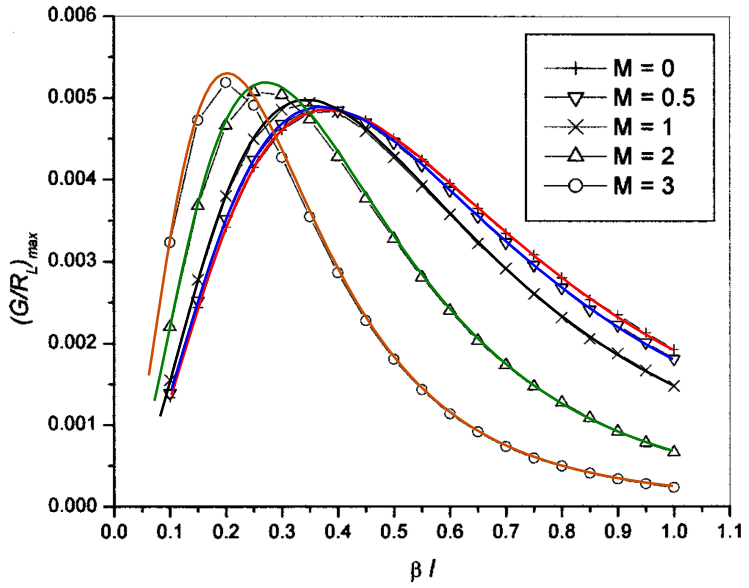

Figure 3. Comparison of present results (thick solid lines) with those of Tumin[17] (markers). Adiabatic wall, spatial analysis, $T_o = 333$ K, $\omega = 0$, $R_\delta = \sqrt{U_e x/\nu_e} = 300$.

For both Mach numbers, the energy amplification $G_{\max}$ features a local maximum for an oblique wave having $\alpha = 0$. This condition corresponds to a streamwise vortex, as is verified by the shape of the optimal disturbance shown in Fig. 5. The disturbance is comprised mainly of vertical and spanwise velocities, with the the temperature fluctuation being substantially smaller and the pressure and streamwise velocity negligible. This form of optimal disturbance has been widely demonstrated for incompressible[5,8] and compressible[17,18] flows alike. By comparison of the two cases in Fig. 5, it is apparent that the shape of the optimal velocity distribution is insensitive to the Mach number. Although the optimal disturbance does contain a noticeable temperature perturbation for the $M = 5$ case, the energy of the disturbance is mostly kinetic: 99.4% of the initial energy is contained in the first three terms of (12).

Figure 6 shows the shape of the optimal perturbation after it has grown to its maximum amplification ($t = t_{opt}$). In this plot the disturbances have been scaled to have a maximum of 1.0, but in fact they have grown by about two orders of magnitude relative to the input disturbance. The amplified disturbance consists mainly of temperature and streamwise velocity, which is consistent with the findings of Hanifi et al.[14] These amplified disturbances take the form of streamwise streaks of alternating high and low velocity and temperature. The physical interpretation of this amplification is the well-known lift-up effect[15,16] in which the streamwise vortices transport low velocity and high temperature (for an adiabatic wall) fluid from the wall towards the outer edge of the boundary layer and vice versa. Although the input disturbances were composed mainly of kinetic energy, after amplification the kinetic energy makes up only 55% (for $M = 2.5$) and 20% (for $M = 5.0$) of the total energy. This demonstrates that the inclusion of the last two terms in (12) has a significant impact on the computed energy growth. A similar distribution of energy amongst its various components was observed by Tempelmann et al.[20]

Table 1. Summary of temporal transient growth characteristics for $R_\delta = 300$.

M_e	T_w/T_e	G_{opt}	T_{opt}	β_{opt}	$\omega_{i,\max}(1^{\text{st}}$ mode)
2.5	2.1 (adiabatic)	437	1030	0.22	9.2×10^{-4}
5.0	5.3 (adiabatic)	483	1150	0.10	5.1×10^{-4}
2.5	1.0	337	750	0.33	0
5.0	1.0	251	897	0.25	0
2.5	0.3	390	602	0.44	0
5.0	0.3	239	770	0.31	0

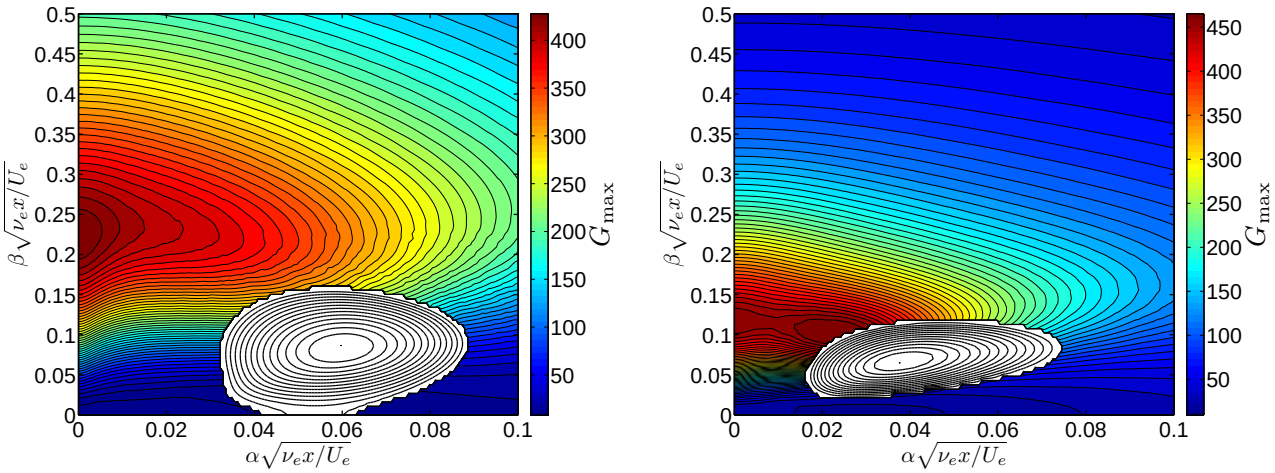

Figure 4. Contours of maximum (temporal) energy amplification $G_{\max}$ vs. streamwise and spanwise wavenumbers. Mach number is 2.5 (left) and 5.0 (right), and $T_w = T_{ad}$, $R_\delta = 300$, $T_e = 70$ K. Colored contours indicate maximum energy amplification, while black contours indicate the growth rate ω_i in regions that are modally unstable. Maximum growth rates in the unstable region are $\omega_i = 9.2 \times 10^{-4}$ for $M = 2.5$ and $\omega_i = 5.1 \times 10^{-4}$ for $M = 5.0$.

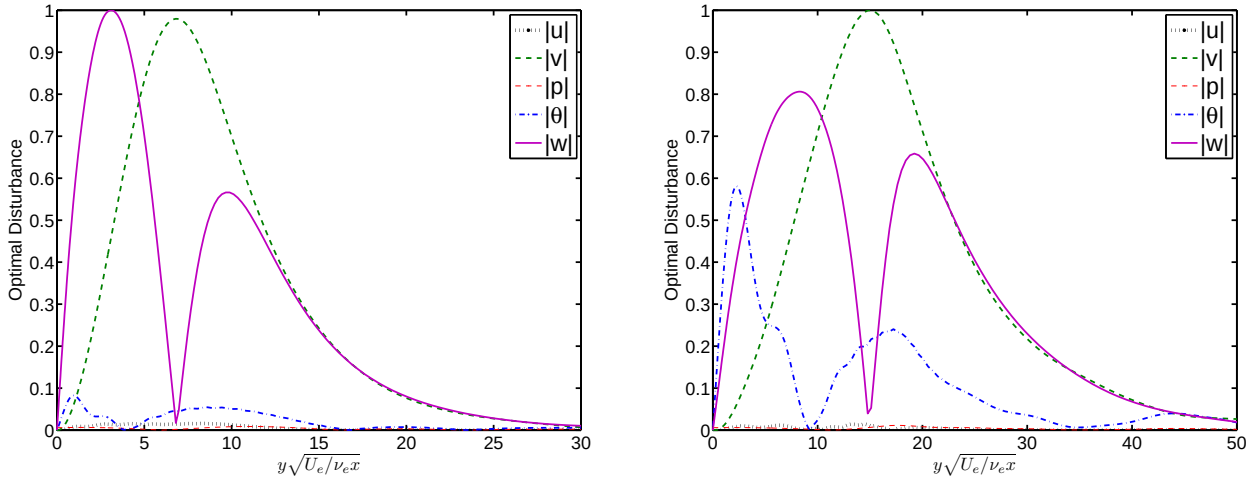

Figure 5. Optimal disturbances corresponding to Fig. 4, $R_\delta = 300$, $T_e = 70$ K, $T_w = T_{ad}$. Left: $M = 2.5$, $\alpha = 0$, $\beta = 0.22$. Right: $M = 5.0$, $\alpha = 0$, $\beta = 0.12$.

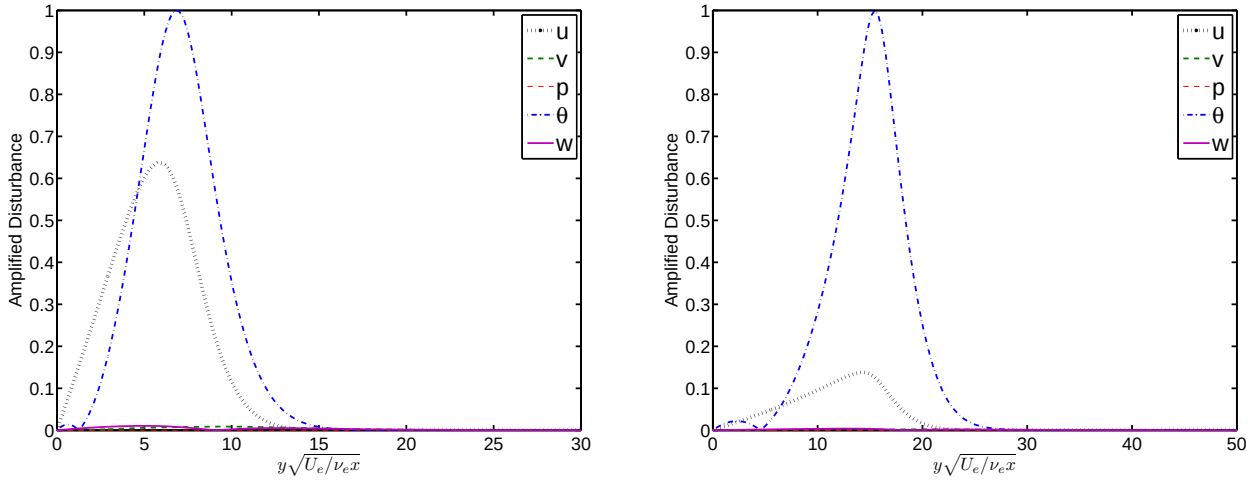

Figure 6. Optimal disturbances after amplification, $t = t_{opt}$, corresponding to Fig. 4. $R_\delta = 300$, $T_e = 70$ K, $T_w = T_{ad}$. Left: $M = 2.5$, $\alpha = 0$, $\beta = 0.22$. Right: $M = 5.0$, $\alpha = 0$, $\beta = 0.12$.

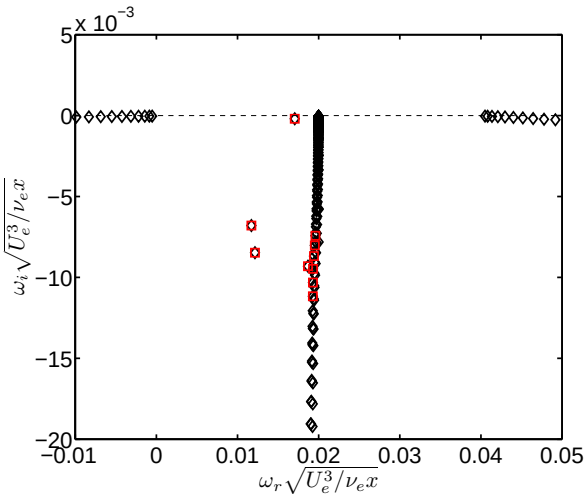

Figure 7. Discrete modes and the discrete approximation to the continuous spectra. $M = 5.0$, $T_w = T_{ad}$, $R_\delta = 300$, $\alpha = 0.02$, $\beta = 0.10$. **Red squares designate the 10 modes that make the largest contribution to the optimal disturbance.**

At $M = 5.0$, Fig. 4 features a second local maximum that borders the first mode instability region, and the energy amplification at this local maximum is slightly larger than at $\alpha = 0$. The optimal disturbance at this condition is composed of the (slightly) damped Tollmien-Schlichting wave combined with several other more highly damped discrete modes as well as modes from the continuous spectra. This is demonstrated in Fig. 7 where the global eigenvalue spectrum is plotted and the 10 modes that contribute most significantly to the optimal disturbance are marked with red boxes. Because of the non-normality of the Navier-Stokes operator, the TS mode and the modes from the vorticity branch interfere destructively such that the initial energy is 1.0 despite the large amplitudes of the modes involved. As time progresses, the modes belonging to the vorticity branch rapidly decay leaving a large-amplitude, slowly-decaying Tollmien-Schlichting mode behind. This process results in a large transient increase in energy. A similar process is always involved in transient growth[38], but this instance is somewhat unique because discrete modes contribute significantly to the transient amplification, rather than modes from the continuous spectrum alone. Interactions of this sort have not been reported in most prior compressible transient growth studies because the perturbations are usually assumed to have $\alpha = 0$ for temporal analyses and $\omega = 0$ for spatial ones. However, there is some similarity between the present result and the "optimally-perturbed TS mode" considered by Farrell[39] and Corbett[21], who sought the initial conditions that produce the largest possible amplitude of Tollmien-Schlichting wave at a later time.

Figure 8 provides contour plots of maximum amplification for a cooled wall with temperature ratio $T_w/T_e = 1.0$; this condition was achieved by setting both the freestream temperature and wall temperature to 300 K. Again, the Mach numbers are 2.5 and 5 and the Reynolds number is $R_\delta = 300$. Owing to the reduction in T_w/T_e relative to the adiabatic case, the first mode instability region is no longer present. There is still a second mode unstable region for $M = 5$, but it is again located at $\alpha > 0.1$ and is not visible in the contour plots. The optimal amplification G_{opt} is somewhat reduced compared to the adiabatic case shown in Fig. 4. Numerically, G_{opt} is reduced by a factor of 1.3 for $M = 2.5$ and a factor of 1.9 for $M = 5$. Also the optimal spanwise wavenumber β_{opt} is increased for $T_w/T_e = 1$, which is a consequence of the thinner boundary layer. By comparison of Figs. 4 and 8, it appears that as the Mach number or level of wall cooling is increased, the transient growth drops off more rapidly away from the optimal condition. That is, near-optimal disturbances are less effective for high Mach numbers and cooled walls.

Figure 9 shows amplification contours for a further reduction in wall temperature relative to the freestream value, $T_w/T_e = 0.3$. In this case the wall temperature is held at 300 K and the freestream temperature is 1000 K, which is representative of a low or moderate enthalpy conditions in a reflected shock facility ($H_o = 2.3$ MJ/kg for $M = 2.5$, 6 MJ/kg for $M = 5$). We have chosen to investigate the effects of wall cooling by raising the freestream temperature rather than by cooling the wall in order to match the conditions found in blowdown facilities and shock tunnels, where the wall temperature is usually ambient. It should be noted that when the ratio T_w/T_e is small (i.e., high edge temperature), this assumption produces slight numerical differences from the results of other researchers who maintain low stagnation temperatures in their

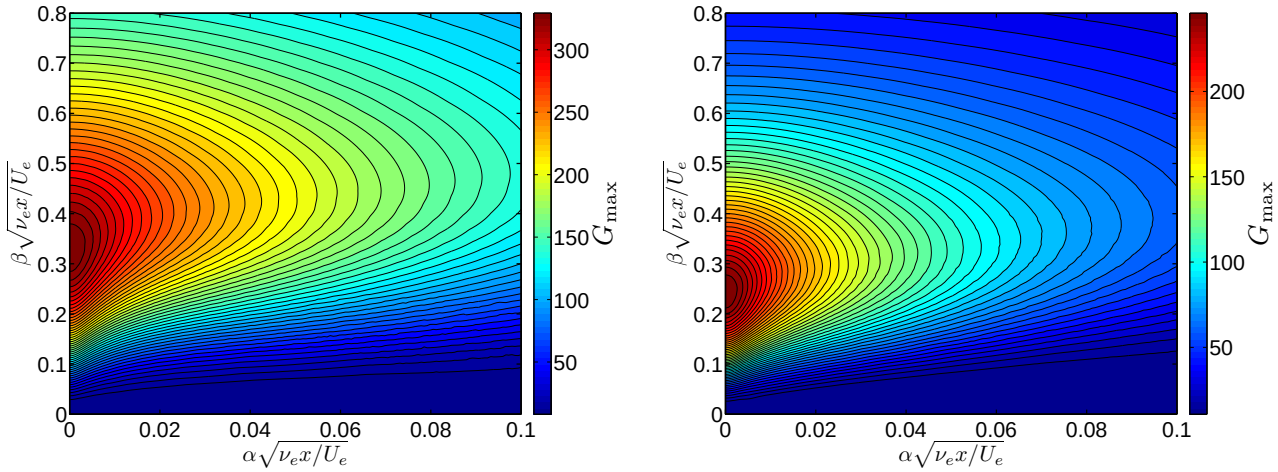

Figure 8. Contours of maximum energy amplification $G_{\max}$ vs. streamwise and spanwise wavenumbers. Mach number is 2.5 (left) and 5.0 (right), and $T_w/T_e = 1.0$, $R_\delta = 300$, $T_e = 300$ K.

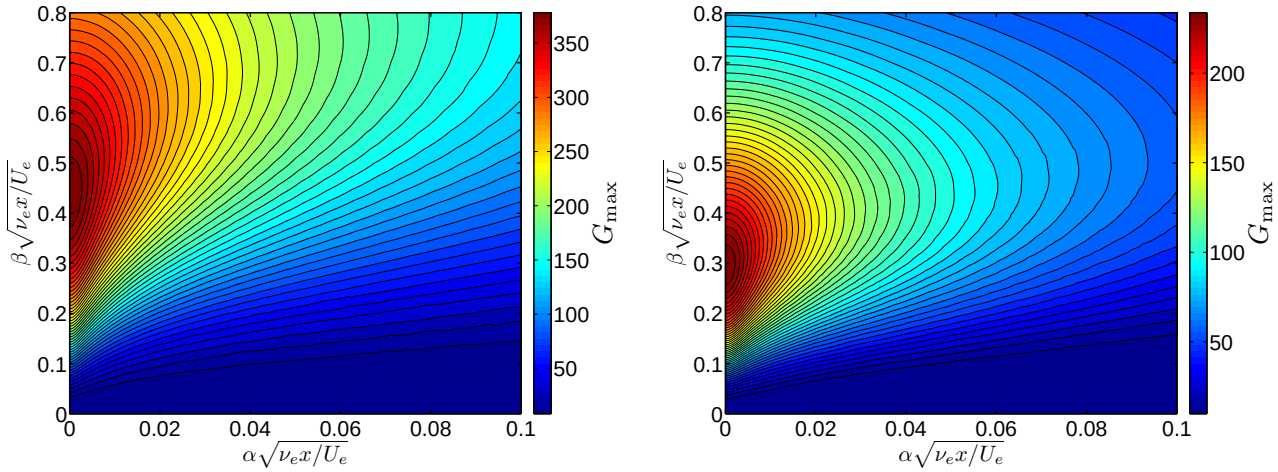

Figure 9. Contours of maximum energy amplification $G_{\max}$ vs. streamwise and spanwise wavenumbers. Mach number is 2.5 (left) and 5.0 (right), and $T_w/T_e = 0.3$, $R_\delta = 300$, $T_e = 1000$ K.

simulations. The numerical differences are caused by the variation of specific heats at high temperature, which we include in our mean flow calculation. Comparison of Fig. 9 to Fig. 8 reveals a further increase in β_{opt} because of the decreased boundary layer thickness caused by wall cooling, but for $M = 5$ there is a slight increase in G_{opt} relative to the case $T_w/T_e = 1$. This suggests that transient growth is minimized for a particular wall temperature condition, as will be verified in the next section.

III.B. Effects of M and Te

The effects of Mach number and wall temperature ratio on the optimal growth were assessed by assembling values of G_{opt} for a large number of different conditions. Different wall temperature ratios were achieved by fixing the wall temperature at 300 K and varying the freestream temperature; as discussed in Sec. III.A, this method was selected in order to match the experimental conditions in impulse facilities. Because of the considerable computational expense of the transient growth calculation, the search for G_{opt} was performed only for $\alpha = 0$ which, as discussed above, is normally where the optimal growth is found. Figure 10 reports values of G_{opt}/R_δ^2 that are optimized over all time, α, and β. This scaling between energy growth and Reynolds number is chosen on the basis of the work by Hanifi et al. [14,29]. The red line with markers indicates the adiabatic wall temperature. Most experimental and flight conditions would fall below this line, but it is possible to conceive of situations in which the wall temperature would be hotter than adiabatic; for instance, a re-entry vehicle that is decelerating from high to low Mach number could experience elevated

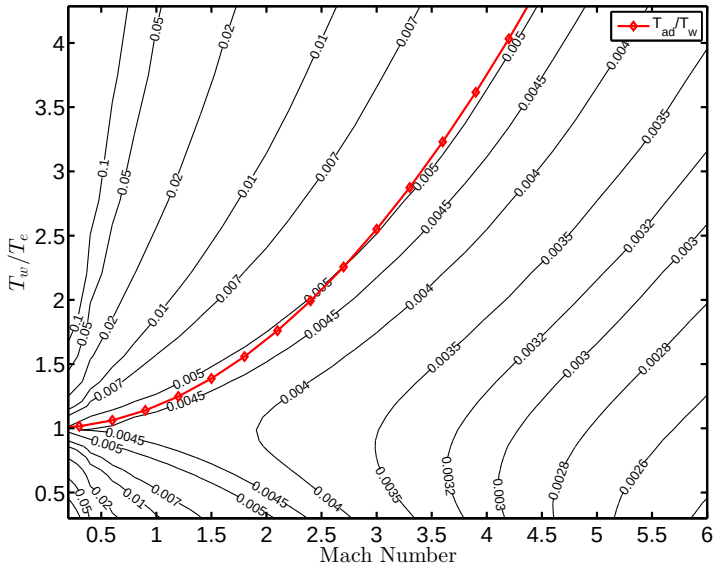

Figure 10. Contours of the maximum possible transient growth vs Mach number and wall temperature ratio. Contour levels represent G_{opt}/R_δ^2 and are optimized over all values of time, α, and β. Red line with markers designates the adiabatic wall temperature. Results were calculated at $R_\delta = 300$.

wall temperatures of this sort.

Figure 10 reveals that the adiabatic line is nearly tangent to an isoline of energy amplification, so if only adiabatic conditions are considered one finds only a slight increase in transient growth as the Mach number is increased, as can be seen in Fig. 3. If the wall is cooled below the adiabatic temperature, however, reductions in amplification can be achieved at high Mach numbers. In particular, as the Mach number is increased there is locus of wall temperature ratios slightly less than 1.0 along which the transient growth is minimized. This minimum in G_{opt}/R_δ^2 is also visible in the results of Tumin and Reshotko[18,28], and the results of the present study are in good agreement with theirs. The agreement is excellent for low Mach numbers, but small numerical differences are found at higher Mach numbers and high levels of wall cooling because of our high stagnation temperature and the variable specific heats which are included in our mean flow calculation.

For low Mach numbers, the influence of wall cooling on the transient growth is substantial. Cooling or heating the wall by a factor of 2.0 results in more than an order of magnitude increase in energy amplification. As noted in the introduction, no modal instabilities exist for low Mach numbers and highly cooled walls, and the route to turbulence under these conditions was questioned. The results of Fig. 10 suggest that transition to turbulence can still be initiated by infinitesimal perturbations since the large density gradients introduced by wall cooling result in high levels of non-modal amplification.

III.C. Temporal vs. Spatial

For convective flows like the boundary layer, the spatial framework is often preferred over the temporal one since it is easier to interpret experimentally. Figure 11 reports transient growth contours for the same conditions as Fig. 4 except that here the spatial framework is used. Both plots in this figure have been generated using the full quadratic eigenvalue problem described in Sec. II.B, and the results do not differ appreciably from those obtained by linearization. Despite the fact that the independent variable is the frequency rather than the wavenumber, the qualitative behavior in the spatial case (Fig. 11) is quite similar to that of the temporal case (Fig 4). Specifically, the energy amplification features a local maximum for an oblique disturbance at $\alpha = 0$ or $\omega = 0$, and the values of G_{opt} and β_{opt} at these conditions are the same. This similarity between the spatial and temporal cases arises from the fact that most of the modes involved in the optimal disturbance belong to the vorticity and entropy branches of the continuous spectrum, for which the phase speed is very nearly 1.0, meaning that the values of α and ω are nearly identical along these branch cuts.

For $M = 2.5$ there is a noticeable difference between the spatial and temporal results, namely, the appearance of a second local maximum in the energy amplification for $\omega > 0$ that is not present in the

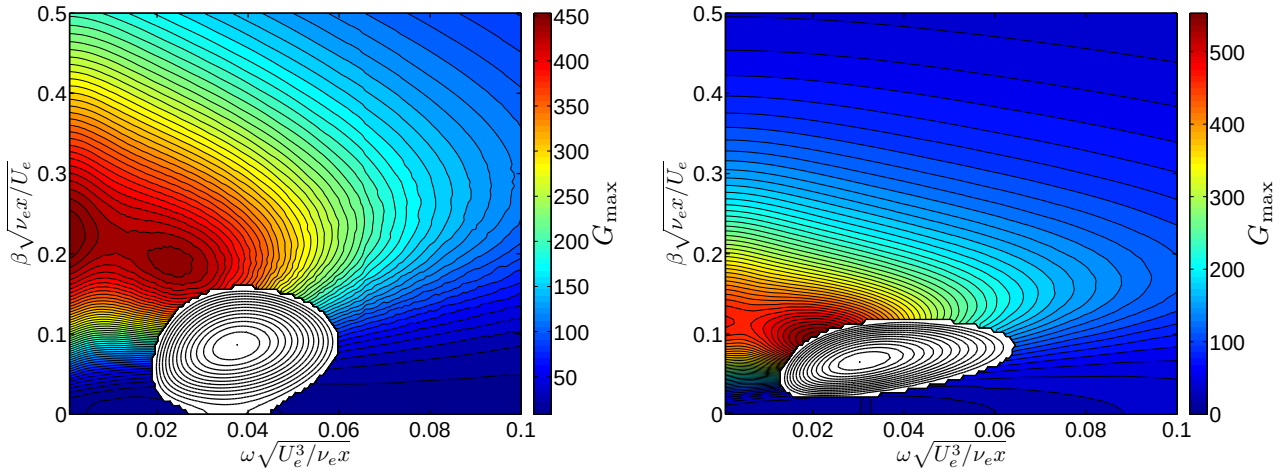

Figure 11. Contours of maximum (spatial) energy amplification $G_{\max}$ vs. streamwise and spanwise wavenumbers. Mach number is 2.5 (left) and 5.0 (right). $T_w = T_{ad}$, $R_\delta = 300$, $T_e = 70$ K. Conditions are the same as in Fig. 4 except that the spatial analysis is used here. The distance x_{opt} at which optimal growth is reached is 790 for $M = 2.5$ and 1150 for $M = 5.0$. For $M = 2.5$, the maximum modal growth rate is $-\alpha_i = 1.3 \times 10^{-3}$ (first mode). For $M = 5$, the maximum growth rates are 5.9×10^{-4} (first mode) and 1.2×10^{-3} (second mode).

temporal case. This second peak at $\omega = 0.022$ has a slightly lower amplification that the one at $\omega = 0$ but develops more rapidly, reaching maximum energy growth at $x = 400$. The optimal disturbance at $\omega = 0$, on the other hand, is maximized at $x = 790$. This demonstrates the fact that slightly sub-optimal disturbances can grow more rapidly than the optimal ones, as will be discussed in the next section.

III.D. Optimization for prescribed downstream distance

As was pointed out by Butler and Farrell[8] and Corbett[21] for incompressible flows, the optimal disturbances take a rather long time to develop. For instance, in Fig. 11 the distance x_{opt} at which the energy is maximized is 790 and 1150 for the respective Mach numbers of 2.5 and 5.0. Recalling that x is normalized by the boundary layer thickness δ, this suggests that the optimal disturbance requires $O(1000\delta)$ to develop. From a modeling standpoint, this fact makes the locally parallel assumption questionable; however, it may be noted that large values of x_{opt} relative to the boundary layer thickness are found in non-parallel simulations as well[5,18]. From a practical standpoint, if x_{opt} is $O(1000\delta)$ it may be unlikely that this distance is reached in a typical laboratory experiment. Moreover, when transient growth requires a large optimization distance, it is less likely that the disturbance will surpass any exponentially growing modal instabilities. These considerations suggest that it may be preferable to maximize the amplification G at a particular distance or time that is relevant to the streamwise length scale of interest rather than optimizing over all possible distances.

Figure 12 provides contours of spatial energy growth G at six fixed distances downstream of the initial disturbance. For each pair of values (α,β), the energy growth G from (16) is calculated at a single, fixed value of x rather than optimizing over all values of x as was done in Figs. 4-9. Although the basic features of the plots in Fig. 12 are similar to those at x_{opt} (Fig. 11), the level of amplification is somewhat lower and the optimal disturbance is no longer found at $\omega = 0$. This is consistent with the (temporal) observation of Butler and Farrell[8] that disturbances having smaller streamwise wavelengths reach their maximum amplitude more rapidly. Although the level of amplification has been reduced relative to the optimal value, the reduction is not always so great as to render the non-modal amplification negligible. For example, at $M = 2.5$ the energy amplification reaches about 2/3 of its optimal value at $x/x_{opt} = 0.25$, which demonstrates that near-optimal amplification can be achieved at distances much less than x_{opt}.

The topology of Fig. 12 is the same as that observed by Corbett and Bottaro for incompressible flow[21]. An isolated peak in G is seen which increases in strength as x is increased. For small x the peak is located at a larger value of ω and approaches $\omega = 0$ as x increases. When x reaches x_{opt} (about 790 for these conditions), the peak value of G is located at $\omega = 0$ and the disturbance takes the form of the optimal streamwise vortex noted in Fig. 5. However, for $x < x_{opt}$ the optimal disturbance is not a streamwise vortex, as shown in Fig. 13 (left). This figure contains the optimal disturbance which produces the peak amplification at $x = 400$ in

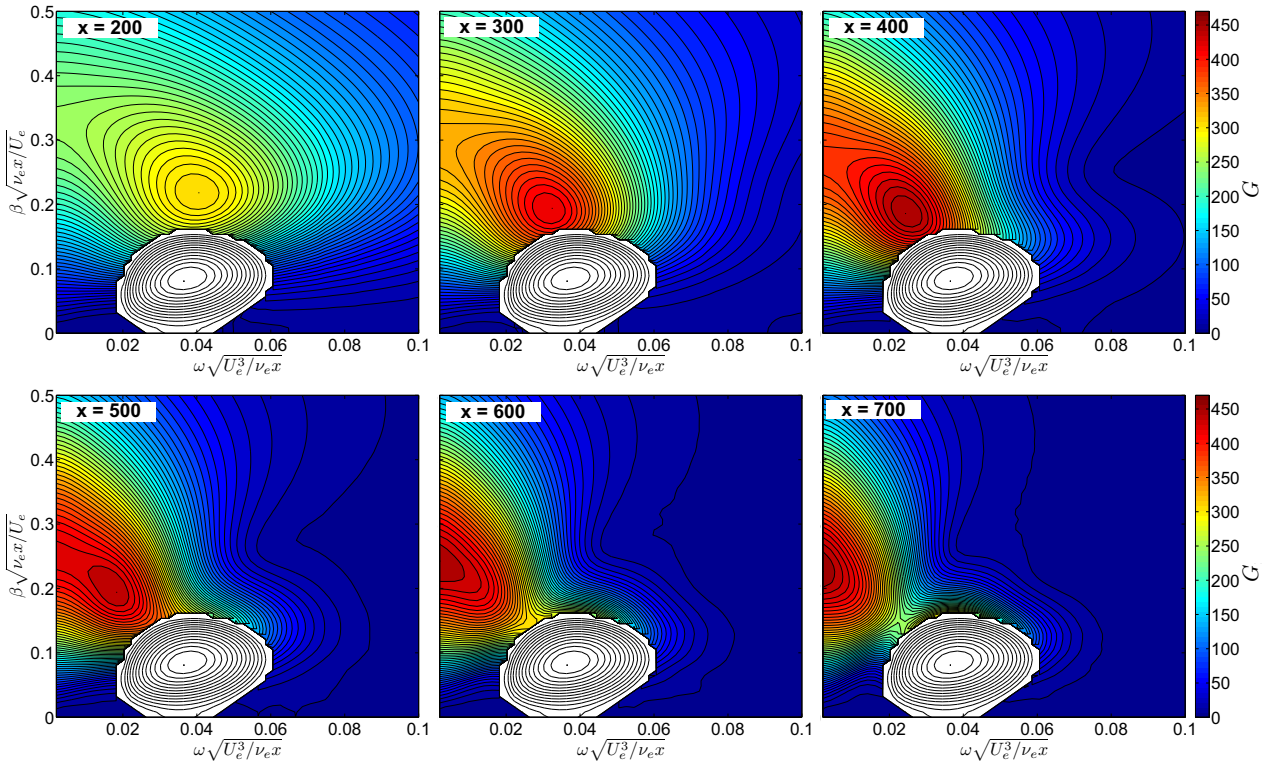

Figure 12. Contours of maximum (spatial) energy amplification G vs. streamwise and spanwise wavenumbers at six different streamwise distances. Mach number is 2.5, adiabatic wall, $R_\delta = 300$, $T_e = 70$ K. Optimal growth is found at $x_{opt} = 790$, $\alpha = 0$,$\beta = 0.22$.

Fig. 12. This initial perturbation evolves into the amplified disturbance shown in Fig. 13 (right) at $x = 400$. As was true in the case of the streamwise vortices in Fig. 6, the amplified disturbance consists of streaks of velocity and temperature, which suggests that the lift up effect is again responsible for the transient growth.

III.E. Modal vs. Non-modal

Our final consideration is a direct comparison between modal and non-modal energy amplification. To minimize the computational expense, we assume $\omega = 0$ in the transient growth calculation, meaning that the optimal perturbation is always a streamwise vortex. Spatial transient growth calculations are carried out for several initial Reynolds numbers, and the downstream evolution of energy for each Reynolds number is compared with the energy growth arising from modal instabilities. For the purposes of comparison, we use the N factor for modal instabilities as defined by:

$$N_{modal}(\omega, \beta) = \int_{x_o}^{x} -\alpha_i(x, \omega, \beta)dx \tag{17}$$

where x_o is the location at which disturbances of frequency ω first become unstable. The analogous N factor for non-modal growth is defined by the relation

$$N_{opt} \equiv \frac{1}{2}\ln(G) \tag{18}$$

where the factor of 1/2 arises from the fact that the energy amplification G scales quadratically with the disturbance amplitude. The definition (18) is chosen by requiring that N_{opt} and N_{modal} be equal when the response consists of a single unstable mode.

An example of the comparison is shown in Fig. 14. Here the Mach number is 2.5 and the wall temperature is adiabatic. The N factors involving transient growth are labeled N_{opt}, and the ten curves correspond to ten different initial Reynolds numbers Re_x between 10^4 and 10^6. For each initial Reynolds number, the optimal disturbance corresponding to the maximum of Fig. 11 ($\alpha = 0$, $\beta = 0.22$) is selected and its downstream

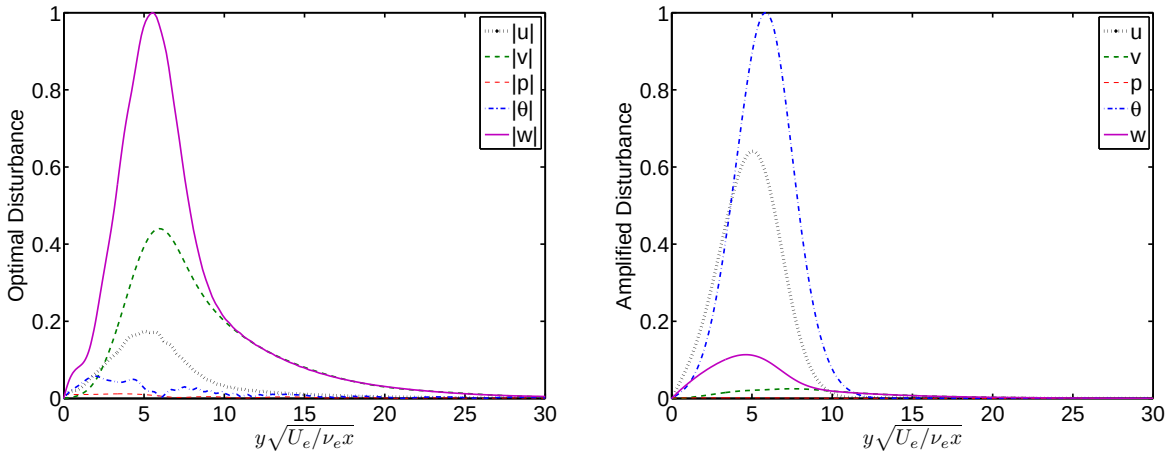

Figure 13. Optimal disturbance for a prescribed downstream distance of $x = 400$. $M = 2.5$, $R_\delta = 300$, $\alpha = 0.025$, $\beta = 0.186$. Left: Optimal disturbance at $x = 0$. Right: Amplified disturbance at $x = 400$.

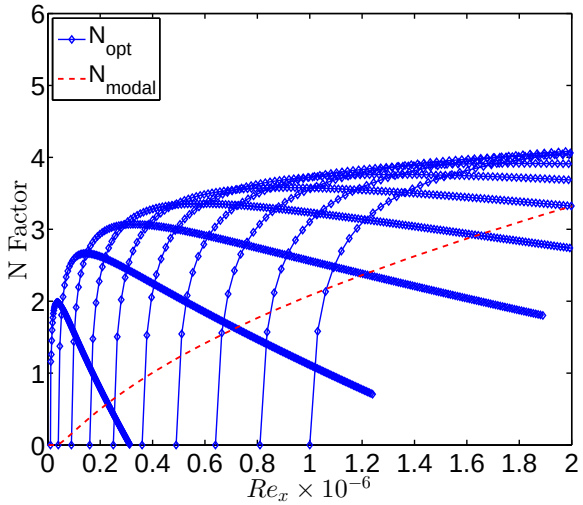

Figure 14. Comparison of N factors from modal and non-modal stability calculations for $M = 2.5$, $T_w = T_{ad}$, $T_e = 70$ K. N_{opt} is the N factor corresponding to non-modal disturbances, N_{modal} is the modal N factor envelope over all values of ω and β.

amplification is calculated. The envelope of these curves marks the maximum level of transient growth that is plausible at each location. The dashed red line represents the envelope of all possible N factor curves corresponding to modal instabilities; this envelope curve is optimized over all frequencies and contains both 2D and 3D disturbances for both the first and second mode instabilities.

For the adiabatic condition shown in Fig. 14, modal growth surpasses non-modal growth at a Reynolds number of about $Re_x = 2.9 \times 10^6$. The N factor at this location is 4.2, which corresponds to an increase in modal amplitude of about 67 and an energy amplification of 4400. This level of amplification is not large, suggesting that under these conditions transition via transient growth might be expected only in a noisy environment where disturbance amplitudes are high, or in situations involving discrete surface roughness elements where strong streamwise, vortical disturbances are likely [28]. However, the level of N at which nonlinear breakdown begins is open to question and may be different for modal and non-modal instabilities, given the differences in the disturbance shapes. The value of N at which transition occurs is also expected to depend on the strength of disturbance sources and the boundary layer's receptivity to them.

Two additional examples of N factor distributions are shown in Fig. 15 which demonstrate the effects of wall cooling. The first example (left) is flow at Mach 5 with a cold wall, $T_w/T_e = 0.3$. This condition might be encountered in a shock tunnel operating at a moderate enthalpy of $H_o = 6$ MJ/kg. In comparison to the low Mach number, adiabatic case shown in Fig. 14, the modal instability overtakes the non-modal one much more rapidly. This is caused by both lower levels of energy amplification and the larger growth rate of the

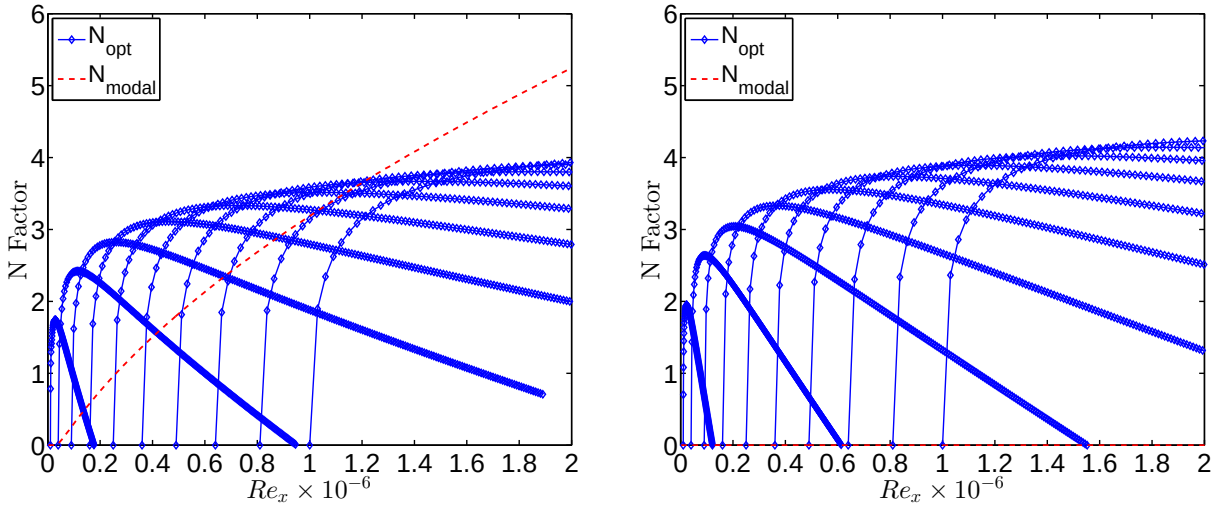

Figure 15. Comparison of N factors from modal and non-modal stability calculations. Left: $M = 5.0$, $T_w/T_e = 0.3$, $T_e = 1000$ **K. Right:** $M = 2.5, T_w/T_e = 0.3$, $T_e = 1000$ **K.**

second mode instability. The modal instability overtakes the transient growth at $Re_x = 1.2 \times 10^6$ where the N factor is 3.7 and the energy amplification is only 1600. Experiments conducted at similar conditions [40] have reported transition at Reynolds numbers of $2 - 3$ million; at this point modal instabilities have undergone more than an order of magnitude larger amplification than non-modal ones.

The second example, Fig. 15 (right), is flow at Mach 2.5 with a cold wall, $T_w/T_e = 0.3$. As discussed in the introduction, there are no modal instabilities for these conditions so the modal N factor is zero. At a Reynolds number of 2.0×10^6, N_{opt} is about 4.2 which corresponds to $G = 4500$. At lower Mach numbers the effect of wall cooling is even greater; for example, at $M = 0.5$ with $T_w/T_e = 0.3$, the N factor at $Re_x = 2 \times 10^6$ is 5.4 and the energy amplification G is 49,000. Moreover, given the well-known [29] scaling $G_{opt} \propto Re_x$, much larger amplification is possible as the Reynolds number is increased. On the basis of this result, it seems reasonable to conclude that flows at low Mach numbers with wall cooling can transition to turbulence from infinitesimal perturbations despite the absence of modal instabilities. In contrast, high Mach number flows with cold wall conditions seem likely to transition by modal mechanisms alone.

IV. Conclusion

This paper investigated the effects of Mach number and wall cooling on the transient growth of disturbances in flat plate boundary layers. Optimal disturbances were calculated in both spatial and temporal frameworks using an eigenvector decomposition of the locally-parallel, linearized Navier-Stokes equations. Both the spatial and temporal frameworks produced similar results in terms of the level of energy amplification, the form of the optimal disturbances, and the optimal spanwise wavenumber. The optimal disturbance was found to consist of streamwise vortices which develop into streamwise streaks of high velocity and temperature. Additional disturbances were found which, though sub-optimal, were highly amplified and grew more rapidly than the optimal ones. Such disturbances were found to have nonzero frequency (or streamwise wavenumber) and did not take the form of streamwise vortices.

For every Mach number, an optimal level of wall cooling was found which minimized the level of transient growth. Although the minimization of transient growth at a particular level of wall cooling can be seen in the results of Reshotko and Tumin [28], the effect of Mach number on this trend was not clear, especially when M is large. The systematic study undertaken in this paper significantly clarifies the roles of Mach number and wall cooling on non-modal amplification. In particular, as $M \to 0$ the transient growth is minimized with no wall cooling, but at high Mach numbers the optimal wall temperature is slightly lower than the edge temperature, and increased wall cooling is needed at higher Mach numbers. Transient growth is found to be especially sensitive to heating or cooling of the wall at low Mach numbers, where a factor of 2 change in wall temperature produces an order of magnitude increase in transient growth.

This paper provides the first direct comparison between modal and non-modal growth in compressible

boundary layers in which integrated N factors are compared for both mechanisms. For conditions relevant to high enthalpy flows (high Mach number, cold wall), modal instability rapidly overtakes the transient growth while the level of amplification is still relatively small (N = 3-4). This suggests that transition to turbulence via transient growth would be significant at these conditions only if the disturbance level is high and the disturbance takes the form of a streamwise vortex, as can be the case for 3D roughness elements. It is also observed that when the Mach number is low and the wall is cooled, no modal instabilities are present and transient growth appears to be the only growth mechanism for infinitesimal perturbations. However, the increased level of transient growth caused by wall cooling under these conditions makes transition by non-modal growth plausible.

Acknowledgments

The authors are grateful to Peter Schmid and Sasha Fedorov for very useful discussions regarding both modal and non-modal instabilities. This work was sponsored in part by AFOSR and NASA through the National Center for Hypersonic Research in Laminar-Turbulent Transition and also by AFOSR award number FA9550-10-1-0491. The views expressed herein are those of the authors and should not be interpreted as necessarily representing the official policies or endorsements, either expressed or implied, of AFOSR or the U.S. Government.

References

[1] Mack, L. M., "Computations of the Stability of the Laminar Compressible Boundary Layer," *Methods in Computational Physics*, edited by B. Alder, S. Fernback, and M. Rotenberg, Vol. 4, Academic Press, New York, 1965, pp. 247–299.

[2] Mack, L. M., "Boundary Layer Stability Theory," Tech. Rep. JPL Report 900-277, Jet Propulsion Lab, California Institute of Technology, 1969.

[3] Mack, L., "Boundary-Layer Linear Stability Theory," *AGARD Report No. 709*, 1984.

[4] Reshotko, E., "Boundary-Layer Stability and Transition," *Annual Review of Fluid Mechanics*, Vol. 8, No. 1, 1976, pp. 311–349.

[5] Andersson, P., Berggren, M., and Henningson, D. S., "Optimal disturbances and bypass transition in boundary layers," *Physics of Fluids (1994-present)*, Vol. 11, No. 1, 1999, pp. 134–150.

[6] Trefethen, L., Trefethen, A., Reddy, S., and Driscoll, T., "Hydrodynamic Stability Without Eigenvalues," *Science*, Vol. 261, No. 5121, 1993, pp. 578–584.

[7] Hultgren, L. S. and Gustavsson, L. H., "Algebraic growth of disturbances in a laminar boundary layer," *Physics of Fluids (1958-1988)*, Vol. 24, No. 6, 1981.

[8] Butler, K. M. and Farrell, B. F., "Three-dimensional optimal perturbations in viscous shear flow," *Physics of Fluids A: Fluid Dynamics (1989-1993)*, Vol. 4, No. 8, 1992, pp. 1637–1650.

[9] Luchini, P., "Reynolds-number-independent instability of the boundary layer over a flat surface," *Journal of Fluid Mechanics*, Vol. 327, 1996, pp. 101–115.

[10] Luchini, P., "Reynolds-number-independent instability of the boundary layer over a flat surface: optimal perturbations," *Journal of Fluid Mechanics*, Vol. 404, 2000, pp. 289–309.

[11] Tempelmann, D., Hanifi, A., and Henningson, D. S., "Spatial optimal growth in three-dimensional boundary layers," *Journal of Fluid Mechanics*, Vol. 646, 2010, pp. 5–37.

[12] Schmid, P. and Henningson, D., *Stability and Transition in Shear Flows*, Springer, New York, 2001.

[13] Reddy, S. C. and Henningson, D. S., "Energy growth in viscous channel flows," *Journal of Fluid Mechanics*, Vol. 252, 1993, pp. 209–238.

[14] Hanifi, A., Schmid, P. J., and Henningson, D. S., "Transient growth in compressible boundary layer flow," *Physics of Fluids*, Vol. 8, No. 3, 1996, pp. 826–837.

[15] Landahl, M. T., "Dynamics of boundary layer turbulence and the mechanism of drag reduction," *Physics of Fluids (1958-1988)*, Vol. 20, No. 10, 1977, pp. S55–S63.

[16] Landahl, M., "A note on an algebraic instability of inviscid parallel shear flows," *Journal of Fluid Mechanics*, Vol. 98, No. 2, 1980, pp. 243–251.

[17] Tumin, A. and Reshotko, E., "Spatial Theory of Optimal Disturbances in Boundary Layers," *Physics of Fluids*, Vol. 13, No. 7, July 2001, pp. 2097–2104.

[18] Tumin, A. and Reshotko, E., "Optimal disturbances in compressible boundary layers," *AIAA Journal*, Vol. 41, No. 12, December 2003, pp. 2357–2363.

[19] Zuccher, S., Tumin, A., and Reshotko, E., "Parabolic approach to optimal perturbations in compressible boundary layers," *Journal of Fluid Mechanics*, Vol. 556, June 2006, pp. 189–216.

[20] Tempelmann, D., Hanifi, A., and Henningson, D., "Spatial Optimal Growth in Three-Dimensional Compressible Boundary Layers," *Journal of Fluid Mechanics*, Vol. 704, August 2012, pp. 251–279.

[21] Corbett, P. and Bottaro, A., "Optimal perturbations for boundary layers subject to stream-wise pressure gradient," *Physics of Fluids (1994-present)*, Vol. 12, No. 1, 2000, pp. 120–130.

[22] Masad, J., Nayfeh, A., and Al-Maaitah, A., "Effect of Heat Transfer on the Stability of Compressible Boundary Layers," *Computers and Fluids*, Vol. 21, No. 1, 1992, pp. 43–61.

[23] Fedorov, A. and Tumin, A., "High-Speed Boundary-Layer Instability: Old Terminology and a New Framework," *AIAA Journal*, Vol. 49, No. 8, August 2011, pp. 1647–1657.

[24] Fedorov, A. and Khokhlov, A., "Prehistory of instability in a hypersonic boundary layer," *Theoretical and Computational Fluid Dynamics*, Vol. 14, No. 6, 2001, pp. 359–375.

[25] Ma, Y. and Zhong, X., "Receptivity of a supersonic boundary layer over a flat plate. Part 1. Wave structures and interactions," *Journal of Fluid Mechanics*, Vol. 488, 2003, pp. 31–78.

[26] Lees, L. and Lin, C., "Investigation of the stability of the laminar boundary layer in a compressible fluid," Tech. Rep. TN-1115, National Advisory Committee for Aeronautics, 1946.

[27] Lees, L., "The stability of the laminar boundary layer in a compressible fluid," Tech. Rep. 876, National Advisory Committee for Aeronautics, 1947.

[28] Reshotko, E. and Tumin, A., "Role of Transient Growth in Roughness-Induced Transition," *AIAA Journal*, Vol. 42, No. 4, April 2004, pp. 766–770.

[29] Hanifi, A. and Henningson, D. S., "The compressible inviscid algebraic instability for streamwise independent disturbances," *Physics of Fluids*, Vol. 10, No. 8, 1998, pp. 1784–1786.

[30] Criminale, W., Jackson, T., Lasseigne, D., and Joslin, R., "Perturbation dynamics in viscous channel flows," *Journal of Fluid Mechanics*, Vol. 339, 1997, pp. 55–75.

[31] Lasseigne, D., Joslin, R., Jackson, T., and Criminale, W., "The transient period for boundary layer disturbances," *Journal of Fluid Mechanics*, Vol. 381, 1999, pp. 89–119.

[32] Klunker, E. and McLean, F., "Effect of Thermal Properties on Laminar-Boundary-Layer Characteristics," Tech. Rep. NACA TN-2916, National Advisory Committee for Aeronautics, 1953.

[33] Vincenti, W. G. and Kruger, C. H., *Introduction to Physical Gas Dynamics*, John Wiley and Sons, New York, 1967.

[34] Malik, M. R., "Numerical Methods for Hypersonic Boundary Layers," *Journal of Computational Physics*, Vol. 86, 1990, pp. 376–413.

[35] Canuto, C., Hussaini, M. Y., Quarteroni, A., and Zang, T. A., *Spectral Methods in Fluid Dynamics*, Springer-Verlag, New York, 1988.

[36] Chu, B., "On the energy transfer to small disturbances in fluid flow (Part I)," *Acta Mechanica*, Vol. 1, No. 3, 1965, pp. 215–234.

[37] Schmid, P. and Henningson, D., "Optimal energy density growth in Hagen-Poiseuille flow," *Journal of Fluid Mechanics*, Vol. 277, pp. 197–225.

[38] Schmid, P., "Nonmodal Stability Theory," *Annual Review of Fluid Mechanics*, Vol. 39, 2007, pp. 129–162.

[39] Farrell, B., "Optimal excitation of perturbations in viscous shear flow," *Physics of Fluids*, Vol. 31, No. 8, 1988, pp. 2093–2102.

[40] Adam, P. H. and Hornung, H. G., "Enthalpy effects on hypervelocity boundary-layer transition: ground test and flight data," *Journal of Spacecraft and Rockets*, Vol. 34, No. 5, September 1997, pp. 614–619.